TESTING OF A WIND TURBINE BLADE SPAR CAP TO WEB JOINT SUBCOMPONENT SUBJECTED TO MULTIAXIAL LOADING

Tobias Laux[1], Riccardo Cappello[1], Jack S. Callaghan[1], Geir Ólafsson[1], Stephen W. Boyd[2], Duncan A. Crump[2], Andrew F. Robinson[2], Ole T. Thomsen[1], Janice M. Dulieu Barton[1,2]

[1] Bristol Composites Institute, School of Civil, Aerospace and Mechanical Engineering, University of Bristol, Bristol, UK
[2] School of Engineering, Boldrewood Innovation Campus, University of Southampton, Southampton, UK

Keywords: Subcomponent testing, T-joint, Digital Image Correlation, Thermoelastic stress analysis

ABSTRACT

A new three-axis subcomponent test set-up was developed to investigate the combined effect of web shear loading and local cross section deformation on the mechanical response and failure behaviour of a composite wind turbine blade spar cap to web T-joint. The representative subcomponent load case was extracted from a Finite Element model of the full blade subjected to pressure to suction side bending. Digital Image Correlation (DIC) and Thermoelastic Stress Analysis (TSA) were employed to capture the deformation of the T-joint specimen. A multicamera DIC system was selected to overcome limitations of a single stereo DIC system in imaging three-dimensional structures. To control and minimise heat convection in the measurement space between the cameras and the structure, fans were used to and shown to improve the DIC results. The novel loading and imaging procedures are developed and demonstrated on a "dummy" steel T-joint specimen with approximately equivalent stiffness to the composite T-joint. The steel T-joint was successfully subjected to realistic multiaxial loading and DIC and TSA results with good signal to noise ratios were obtained. A description of the test set up for the composite joint is provided based on the experience gained on the steel joint.

1 INTRODUCTION

The design and certification approach for wind turbine blades (WTBs) currently relies on material properties derived experimentally on the coupon scale to predict design allowables at the structural scale, and on full-scale validation testing [1]. The former necessitates the application of conservative knock-down factors, as the failure modes do not readily scale, and the latter is prohibitively expensive, requiring large, specialised facilities. Full-scale validation tests will continue to be essential to ascertain if a blade can withstand the design loads within the prescribed levels of confidence. However, as full-scale tests are costly and require large timescales to run, they are unsuitable for validation of the design during a blade design and development programme. Further they are not suitable for detailed investigations of local failure phenomena [2]. Similarly, coupon scale testing will for the foreseeable future be required to inform analysis frameworks at higher length scales, but they are not sufficiently complex and representative to investigate structural scale failure modes. Consequently, the efficient, low risk, and cost-effective exploration of new materials and structural concepts for WTBs is inhibited by the current certification practice. With the increasing size and complexity of WTBs it is therefore desirable to move towards a design and certification approach that includes experiments at the subcomponent level. In the aerospace sector, this building block or 'testing pyramid' approach has been used for decades [3] with the primary aim to mitigate risk by validating the design and analysis tools continuously on increased levels of complexities and associated costs.

While the potential of WTB subcomponent testing is recognised [2], [4], research on the subcomponent level is relatively sparce due to the cost and challenges associated with the manufacture of large and complex test articles, the need for bespoke loading frames, and specialised data measurement systems. Therefore, no consensus has been reached on the most promising candidates for subcomponent testing, and the design and implementation of such tests. Examples of WTB subcomponent testing include the investigation of the failure behaviour of a grid-scored foam cored

sandwich panel (part of the WTB aerodynamic shell) subjected to realistic combined biaxial tension-tension-bending and compression-compression-bending [5], the investigation of compressive trailing edge failure triggered by global edge-wise bending of the blade [6], [7], and the assessment of a spar cap to web bonded joint using a cantilever beam bending test [8]. The research in [5]–[8] demonstrates how subcomponent testing can provide critical information on the structural response and failure modes of WTBs that cannot be obtained using coupon or full-scale testing.

The aim of the work described in the paper is to develop a subcomponent testing methodology to investigate the combined effect of web shear loading and local cross section deformations induced by the Brazier effect [9] on the spar cap to web T-joint in a single shear web WTB design subjected to pressure to suction (PTS) side (or flap wise) bending, as shown in Figure 1 (a). Composite T-joints have been studied experimentally extensively, e.g. [10], [11], but were mainly conducted on two-dimensional T-joints that does not account for the effect of web shear loading. Furthermore, the experimental set-ups normally comprise a single actuator pushing, pulling, or bending the shear web, while the ends of the flange are fixed. These load cases do not accurately represent the cross section deformation induced into a WTB spar cap to web joint, as predicted by Finite Element (FE) models and shown in Figure 1 (b). Consequently, the failure modes observed in previous T-joint tests [10], [11] are not representative. Therefore, a bespoke three-axis test rig has been designed that allows more representative loading scenarios to be applied to a spar cap to web T-joint. The test set-up is specified for a 1.2 m long T-joint section at the pressure side of the blade centred around a cross section located at 21 m radial distance from the WTB root, as indicated in Figure 1 (a). A further objective of the work is the exploitation of full-field imaging techniques such as Digital Image Correlation (DIC) [12] and Thermoelastic Stress Analysis (TSA) [13] based on thermal images captured by infrared (IR) cameras for the structural assessment of subcomponents.

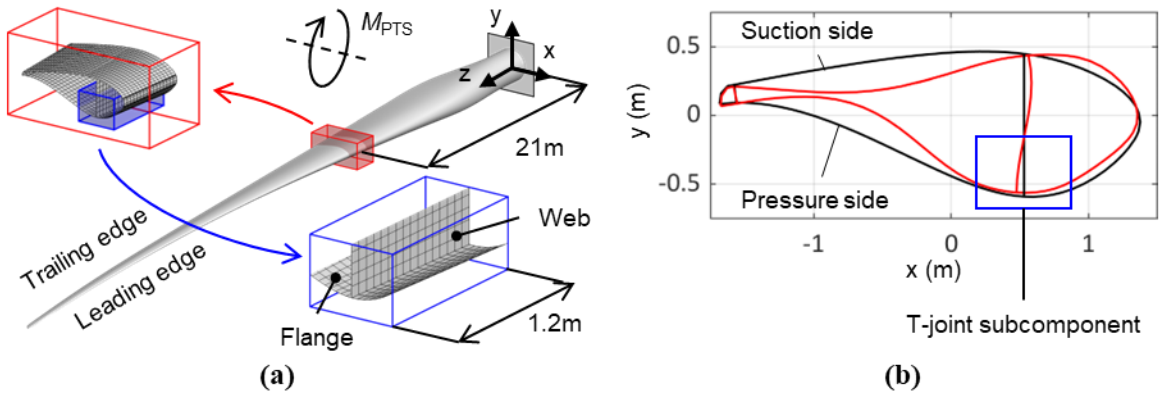

Figure 1: Spar cap to web joint subcomponent: (a) definition of subcomponent and pressure to suction (PTS) bending load case, and (b) cross section deformation at the location of the subcomponent extracted from an FE model of the full WTB.

As only two composite T-joints were available for testing, a dummy T-joint specimen made from steel with approximately equivalent stiffness to the composite specimen was used to develop and commission the novel loading and imaging procedures. The paper contains a description of progress on the steel T-joint testing and evaluation which informs the development of the composite T-joint as well as further subcomponent testing campaigns.

2 EXPERIMENTAL SET-UP

2.1 Loading rig

A FE model of the full blade provided the shell resultants and deformations of the subcomponent, as shown in Figure 1 (b), based on which an experimental subcomponent testing set-up was devised that generated similar deformations in the test specimen [14]. The final three-axes test set-up is shown schematically in Figure 2 (a). The unique characteristics of the set-up are firstly the three dimensional

nature of the T-joint that allows the application of web shear loading via the horizontal actuator 3, and secondly the pinned connection at the web edge that is crucially important to allow for the curvature inflexion point in the deformed web (red in Figure 1 (b)). The inflexion point is associated with a zero transverse bending moment and a transition from positive to negative web bending. Only a pinned web edge connection at the location of the zero transverse bending moment enables realistic cross sectional T-joint subcomponent loading and was therefore incorporated in the set-up. Lastly, the two vertical actuators 1 and 2 in Figure 2 enable the application of the cross section deformation, mainly consisting of flange and web bending and web compression.

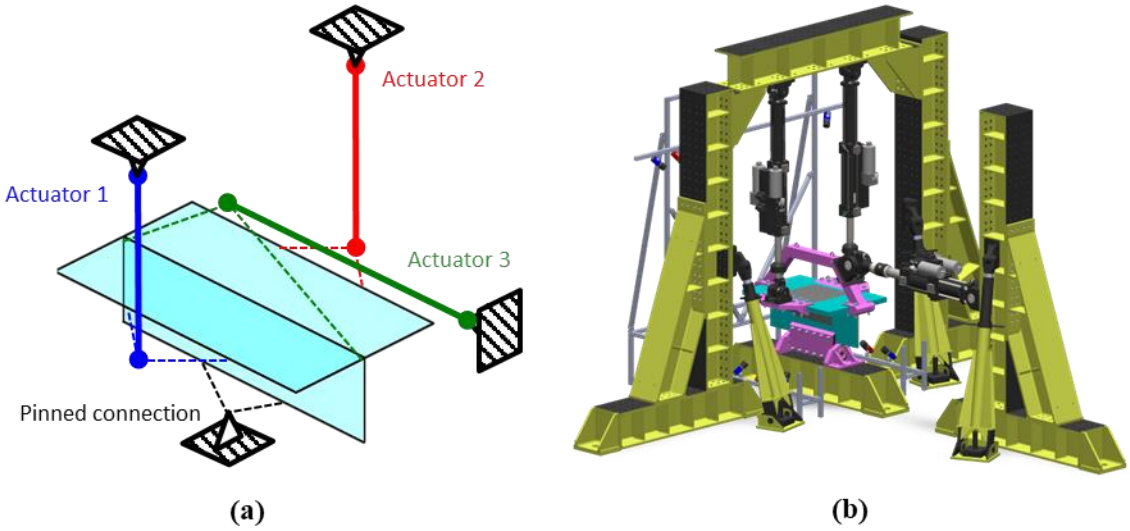

Figure 2: Experimental three-axis loading configuration: (a) test schematic, (b) detailed CAD assembly of test set-up.

Once the loading configuration was defined, the detailed experimental arrangement was specified, as shown in Figure 2 (b). The experiment uses the Structures 2025 test facility which is installed on the strong floor of the Large Structures Testing Laboratory (LSTL) at the University of Southampton. Generic modular loading frames (yellow and black members in Figure 2 (b)) are used alongside bespoke specimen clamps (purple in Figure 2 (b)). The loading is applied with two vertical MTS 244.22G2 100kN actuators and a horizontal MTS 244.31G2 250kN actuator controlled by an MTS FlexTest 200 system. While the testing set-up considers interaction effects of web shear loading and cross section deformation, it does not account for other dominant stresses in the vicinity of the T-joint that are predicted by the FE model, such as the blade bending induced longitudinal normal stresses in the flange, and the blade torsion induced flange shear stresses.

2.2 Full-field imaging systems

To monitor the load response, the underside of the T-joint is imaged using DIC, as shown in Figure 3. The underside was chosen, because in preliminary tests on a composite T-joint, the stress and strain response from the top side of the flange was very low in comparison to that obtained from the underside near the joint. Failure is therefore expected to be observed on the underside rather than the topside. The region of interest, as shown in Figure 3 (a), was sprayed with Electrolube matt black paint, and white speckles were applied using ambersil acrylic matt white spray paint. The speckles were applied using a dotted stencil that was laser cut from 3mm thick plywood. The cutting file was computer generated and allows the application of speckle patterns with controlled speckle size and density. As the steel T-joint specimen used in this work is a precursor for the composite specimen with the aim to optimise the loading and imaging procedures, a fine and coarse speckle pattern were applied, as shown in Figure 3 (a), to investigate its influence on DIC system performance. To image web and flange regions of the T-joint specimen with a single stereo DIC system is challenging: it not only requires a large depth of field, which in turn rises the requirements for lighting, but the highly oblique angles between the

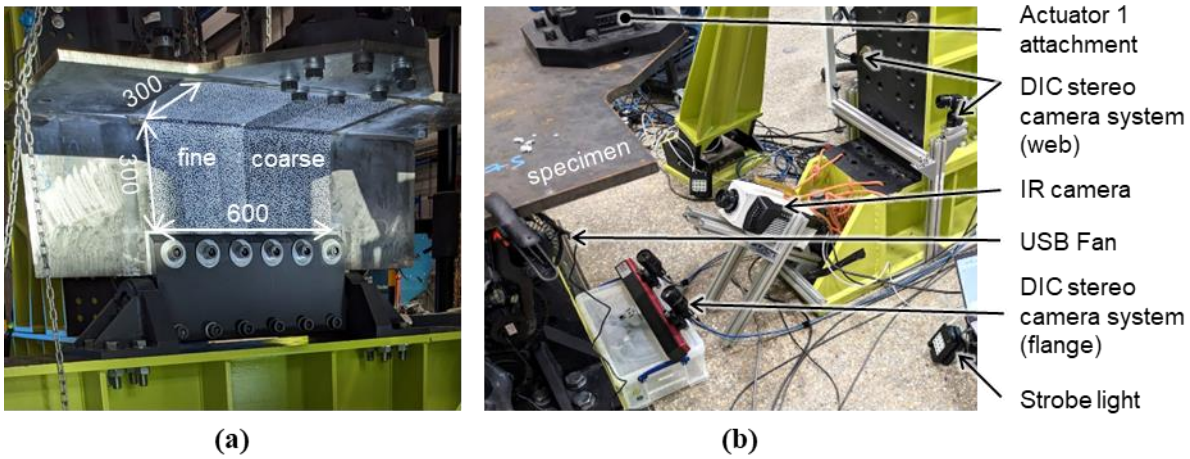

Figure 3: Full-filed imaging systems set-up: (a) gauge zone with speckle pattern, and (b) white light cameras, lights, and fan for DIC, and IR camera for TSA. Dimensions in mm.

speckled surfaces and the camera sensors also distort the subsets and complicate pattern matching between the two cameras, which can result in uncorrelated areas [15]. For this reason, two individual stereo systems were used to image the web and the flange regions individually, as shown in Figure 3 (b), enabling them to be positioned perpendicular to the imaged surfaces. All four white light cameras were Flir Blackfly 8.9 MPx cameras. The stereo pair imaging the web was equipped with Computar 25 mm, 1.1", C-mount lenses, while the stereo pair imaging the flange was equipped with Computar 12 mm, 1.1", C-mount lenses. Two GSVitec high power LED lights were positioned on the ground on both sides of the measurement space, as indicated in figure 3 (b). They were controlled by a MultiLed GX8 controller in strobing mode synchronised with the MatchID trigger box [16].

Initial imaging trials revealed poor DIC system performance, especially manifesting itself in high noise levels in the strain fields in excess of 300 με. Taking images of the static specimen at a relatively high frame rate of 10 Hz revealed patterns in the strain fields akin to patterns of convective air currents, or heat waves, that form due to temperature gradients in the measurement space [17]. Imaging an object through heat waves can lead to significant shape distortions due to the different refractive indices of cold and hot air, which in turn affects the derived displacement and strains. In the present experiment, heat convection is likely to be augmented by the relatively hot lights positioned in a large and open testing hall with no environmental control. Following the recommendation given in [17] a fan was used to mix the air to achieve a more homogeneous temperature distribution in the measurement space. Even though the fan cannot completely alleviate the effect of heat convection, it significantly reduced the noise levels in the strain fields to acceptable levels less than 100με. Another measure to reduce convection was the use of strobe lights instead of the commonly used continuous lighting to minimise the heating of the cameras. The commercial DIC software MatchID was used for image capture and processing. Furthermore, MatchID's Multicamera module was used to transform the results from the web and flange stereo camera pairs into a common global coordinate system.

Lastly, a Telops Mk2 FAST-IR photon detector was installed centrally, as shown in Figure 3 (b), imaging the whole region of interest.

2.3 Testing and imaging procedure

The testing procedure is illustrated in Figure 4 and consist of incremental F_1=5 kN loading blocks (after an initial 10 kN loading block) to ensure sufficient data can be collected to provide a detailed insight into the structural behaviour before failing the limited number of specimens. The constant load regions of the loading blocks represent the PTS side blade bending subcomponent load case as determined from the FE model with a ratio of $R=F_3/F_1=0.833$. White light images for DIC are taken at a frame rate of 0.5 Hz during the loading ramp (0.1kN/s), the hold period once the load levels are reached, and during the ramp down. Each hold period contained at least 10 images for DIC to enable correlation of averaged images (indicated by the lime green blocks in Figure 4), which reduced the effect

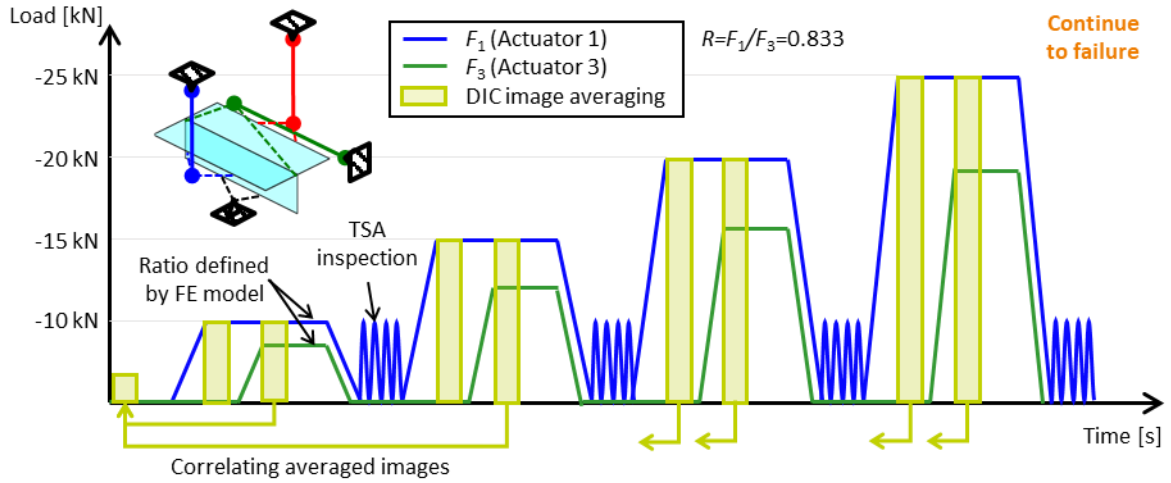

Figure 4: Loading and imaging procedure for the first four load levels investigated on the steel T-joint specimen.

of camera sensor noise and heat waves on the displacement and strain measurement resolution. So far, the steel T-joint has been loaded up to F_1=25 kN, but the process will be continued until the T-joint fails.

After each loading block, the specimen was inspected using TSA, which requires imaging the specimen with an IR camera during cyclic loading (annotated in Figure 4). In this manner, the thermoelastic response of the T-joint can be assessed after each loading block, where changes in the distribution of the sum of principal stresses (derived using TSA based on IR images) will indicate the onset of inelastic behaviour (or damage).

3 EXPERIMENTAL RESULTS AND DISCUSSION

The DIC results obtained by the multicamera set-up, using strobe lights and mixing fans, in combination with the image averaging approach described in the previous section, are shown in Figure 5. The deformed shapes of the T-joint subjected to the loading profile in Figure 4 are shown in Figure 5 (a); it can be observed that the specimen undergoes a rigid rotation around the pinned

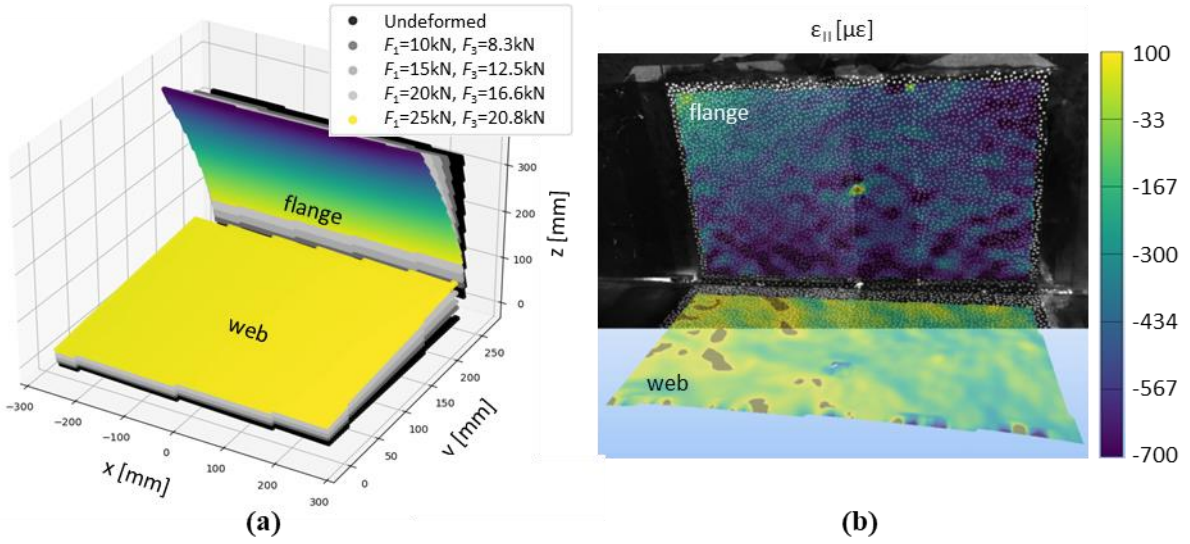

Figure 5: DIC results for the steel T-joint specimen: (a) evolving deformation x 10 with increasing load F_1 and F_3, and (b) ε_{II} strain map at F_1=25kN and F_3=20.8kN as seen through the right hand side camera pointed at the flange.

connection of the web in combination with flange bending. Figure 5 (b) shows the minimum principal strain map, ε_{II}, corresponding to the last investigated load case at F_1=25 kN. The strain map reveals compressive ε_{II} stresses in the flange with an absolute maximum of just over 700 με close to the joint line. In comparison to the flange, the web only undergoes minor bending. Overall, there is a strong signal to noise ratio in both the displacement and strain fields that clearly enables identification of dominant deformation modes, specimen misalignment, and evolving strain concentrations that indicate inelastic deformation, or damage.

4 CONCLUSIONS AND FUTURE WORK

A novel testing set-up has been developed and commissioned for the investigation of a WTB spar cap to web T-joint specimen subjected to combined web shear and cross section deformation. The set-up is unique due to the three-dimensional nature of the T-joint specimen, allowing the application of web shear loading, and the pinned web edge boundary condition, which is required to accurately capture the cross-section deformation of the wind turbine blade subjected to PTS side bending. A steel T-joint dummy specimen was used to develop and optimize the new loading and imaging procedures and to conduct initial trials of the actuator control and data acquisition systems. A DIC imaging set-up has been devised to monitor the underside of the T-joint specimen using two stereo DIC systems to overcome limitations of single stereo DIC in imaging three dimensional structures. Moreover, fans to mix the air in the measurement space and strobe lights have been shown to alleviate heat wave effects on the DIC results, and good signal to noise ratios have been achieved. Furthermore, TSA was used as an inspection technique with the aim of associating the occurrence of inelastic deformation or onset of damage to changes in the thermoelastic response.

Future work will include the loading of the steel T-joint specimen up to failure. The DIC and IR imaging systems will be used, in a practically identical manner to that described above to capture the onset of damage. The imaging data will be compared to FE model predictions to verify the selection of FE boundary conditions. Following on from this, the composite T-joint specimen will be prepared and installed in the Structures 2025 facility using an identical set-up to that described above. Using the validated loading and imaging procedures described in the present paper, the composite T-joint will be loaded to failure. The test result will generate new knowledge on the failure of composite T-joints subjected to realistic WTB loading conditions and will advance the state-of-the-art in data-rich subcomponent testing.

ACKNOWLEDGEMENTS

This research was supported by the EPSRC Programme Grant ‘Certification for Design – Reshaping the Testing Pyramid’ (CerTest, EP/S017038/1), and the EPSRC Equipment Grant ‘Structures 2025: A High Fidelity, Data Rich, Paradigm Shift For Structural Testing’ (EP/R008787/1). The experiments were conducted in the Large Structures Testing Laboratory (LSTL), which is part of the UKCRIC National Infrastructure Laboratory (NIL), based at the University of Southampton. The help of Andrew Morgan, LSTL Technician, in setting-up the experiment is gratefully acknowledged.

REFERENCES

[1] DNV-GL, “DNV-ST-0376 Rotor blades for wind turbines.” 2021.

[2] A. Antoniou, K. Branner, D. J. Lekou, I. Nuin, and R. Nijssen, “Methodology for testing subcomponents; background and motivation for subcomponent testing of wind turbine rotor blades,” 2016.

[3] J. Rouchon, “Certification of large aircraft composite structures, recent progress and new trends in compliance philosophy,” in *17th ICAS Congress*, Stockholm, 1990, pp. 1439–1447. [Online]. Available: http://www.icas.org/ICAS_ARCHIVE/ICAS1990/ICAS-90-1.8.1.pdf

[4] M. Rosemeier, G. Basters, and A. Antoniou, “Benefits of subcomponent over full-scale blade testing elaborated on a trailing-edge bond line design validation,” *Wind Energy Science*, vol. 3, no. 1, pp. 163–172, 2018, doi: 10.5194/wes-3-163-2018.

[5] S. Laustsen, E. Lund, L. Kühlmeier, and O. T. Thomsen, "Development of a high-fidelity experimental substructure test rig for grid-scored sandwich panels in wind turbine blades," *Strain*, vol. 50, no. 2, pp. 111–131, 2014, doi: 10.1111/str.12072.
[6] F. Lahuerta, N. Koorn, and D. Smissaert, "Wind turbine blade trailing edge failure assessment with sub-component test on static and fatigue load conditions," *Compos Struct*, vol. 204, no. March, pp. 755–766, 2018, doi: 10.1016/j.compstruct.2018.07.112.
[7] M. Rosemeier, A. Antoniou, X. Chen, F. Lahuerta, P. Berring, and K. Branner, "Trailing edge subcomponent testing for wind turbine blades–Part A: Comparison of concepts," *Wind Energy*, vol. 22, no. 4, pp. 487–498, 2019, doi: 10.1002/we.2301.
[8] G. Fernandez, H. Usabiaga, and D. Vandepitte, "Subcomponent development for sandwich composite wind turbine blade bonded joints analysis," vol. 180, pp. 41–62, 2017, doi: 10.1016/j.compstruct.2017.07.098.
[9] L. G. Brazier, "On the flexure of thin cylindrical shells and other 'thin' sections," *Proceedings of the Royal Society of London. Series A, Containing Papers of a Mathematical and Physical Character*, vol. 116, no. 773, pp. 104–114, 1927, doi: 10.1098/rspa.1927.0125.
[10] R. A. Shenoi, P. J. C. L. Read, and G. L. Hawkins, "Fatigue failure mechanisms in fibre-reinforced plastic laminated tee joints," *Int J Fatigue*, vol. 17, no. 6, pp. 415–426, 1995, doi: 10.1016/0142-1123(95)98238-X.
[11] Y. Wang and C. Soutis, "A Finite Element and Experimental Analysis of Composite T-Joints Used in Wind Turbine Blades," *Applied Composite Materials*, vol. 25, no. 4, pp. 953–964, 2018, doi: 10.1007/s10443-018-9711-3.
[12] M. A. Sutton, J. J. Orteu, and H. Schreier, *Image correlation for shape, motion and deformation measurements*. Springer, 2009.
[13] J. M. Dulieu-Barton, "Introduction to thermoelastic stress analysis," *Strain*, vol. 35, no. 2, pp. 35–39, 1999, doi: 10.1111/j.1475-1305.1999.tb01123.x.
[14] J. S. Callaghan, "High fidelity testing of wind turbine blade substructures," PhD Thesis, University of Southampton, 2022.
[15] P. Reu, "Stereo-rig Design: Stereo-Angle Selection — Part 4," *Exp Tech*, vol. 37, pp. 1–2, 2013.
[16] "MatchID." [Online]. Available: https://www.matchid.eu/
[17] E. M. C. Jones and P. L. Reu, "Distortion of Digital Image Correlation (DIC) Displacements and Strains from Heat Waves," *Exp Mech*, vol. 58, no. 7, pp. 1133–1156, 2018, doi: 10.1007/s11340-017-0354-3.